Physica E 151 (2023) 115711

Contents lists available at ScienceDirect

Physica E: Low-dimensional Systems and Nanostructures

journal homepage: www.elsevier.com/locate/physe

Subwavelength confinement of a quantum emitter in ladder configuration adjacent to a nanostructured plasmonic metasurface

Hamid R. Hamedi [a,*], Viktor Novičenko [a], Gediminas Juzeliūnas [a], Vassilios Yannopapas [b], Emmanuel Paspalakis [c]

[a] Institute of Theoretical Physics and Astronomy, Vilnius University, Saulėtekio 3, Vilnius LT-10257, Lithuania
[b] Department of Physics, School of Applied Mathematical and Physical Sciences, National Technical University of Athens, GR-157 80 Athens, Greece
[c] Materials Science Department, School of Natural Sciences, University of Patras, Patras 265 04, Greece

ARTICLE INFO

Keywords:
Subwavelength localization
Plasmonic nanostructure
Ladder light matter coupling

ABSTRACT

We theoretically demonstrate the subwavelength confinement of a quantum emitter in ladder configuration adjacent to a plasmonic nanostructure. The lower leg of the ladder system interacting with a weak probe beam of light is far detuned from the surface of the plasmonic nanostructure and thus does not feel any effect from the plasmonic nanostructure. On the other hand, the upper, V-type, leg coupling with a standing wave (SW) control field interacts with the surface-plasmon bands of the nanostructure, giving the anisotropic Purcell effect to the spontaneous emission and leading to quantum interference in the spontaneous emission. The application of the SW beam makes the light-matter interaction spatially dependent, as a result, measuring the absorption of the weak probe beam provides a suitable tool to acquire information about the spatial confinement of the emitter. It is found that when the nanostructure system is present, the spatial distribution of probe absorption modifies significantly, allowing a distant control of subwavelength localization of the quantum emitter. In particular, a superlocalization regime can be achieved for emitter-metasurface separation distances from $0.65c/\omega_p$ to c/ω_p.

1. Introduction

Light–matter interaction engineering has been an appealing field of research with interesting consequences implemented in chemistry, physics and nanotechnology [1]. Restricting light to nanosize volumes through interacting with the conduction electrons of nanostructures has been shown to result in various significant effects [2–4]. In addition, quantum coherence and quantum interference in emitters placed near the nanostructured plasmonic metasurface has led to several phenomena, for instance the transparency and resulting slow light [5–7], enhancement in the index of refraction [8], Fano effects in energy absorption [9,10], modification of spontaneous emission [11–13], coherent control of the optical bistability [14–16], four-wave-mixing [17,18], enhanced Kerr nonlinearity [19,20], amplification without inversion [21–23], and so on [24–27].

On the other hand, confinement in space of single emitters (mainly atoms) has received a considerable interest because of its application possibilities in patterning of Bose–Einstein condensation [14,28], laser cooling [29], center-of-mass wave function measurements [30], and atom nanolithography [31]. Different optical-based methods have been proposed for spatial confinement of emitters [32–49]. These techniques are mainly based on the dark state of coherent population trapping (CPT) [37] or Stimulated Raman Adiabatic Passage (STIRAP) [43], detection of spontaneously emitted photon [45], measuring the spatial distribution of either excited state population [33] or probe field absorption [32,36].

While most of previous studies on subwavelength localization have dealt with single emitters in vacuum, a remote distant control of subwavelength localization of an emitter placed next to a periodic plasmonic nanostructure has motivated this study. To this end, here we consider a ladder shaped quantum emitter characterized by four energy levels which is located next to the surface of a plasmonic nanostructure. Specifically, a weak probe laser field acts on the lower leg of the ladder configuration which is not influenced by the nanostructure. On the other hand, the upper, V-type, leg interacting with a standing wave (SW) beam (control field) exists in the surface-plasmon bands of the nanostructure, giving the anisotropic Purcell effect to the spontaneous emission and leading to quantum interference in the spontaneous emission [11]. As a result, the light-matter interaction becomes space-dependent when the quantum system interplays with

* Corresponding author.
E-mail addresses: hamid.hamedi@tfai.vu.lt (H.R. Hamedi), viktor.novicenko@tfai.vu.lt (V. Novičenko), gediminas.juzeliunas@tfai.vu.lt (G. Juzeliūnas), vyannop@mail.ntua.gr (V. Yannopapas), paspalak@upatras.gr (E. Paspalakis).

https://doi.org/10.1016/j.physe.2023.115711
Received 30 October 2022; Accepted 18 March 2023
Available online 30 March 2023

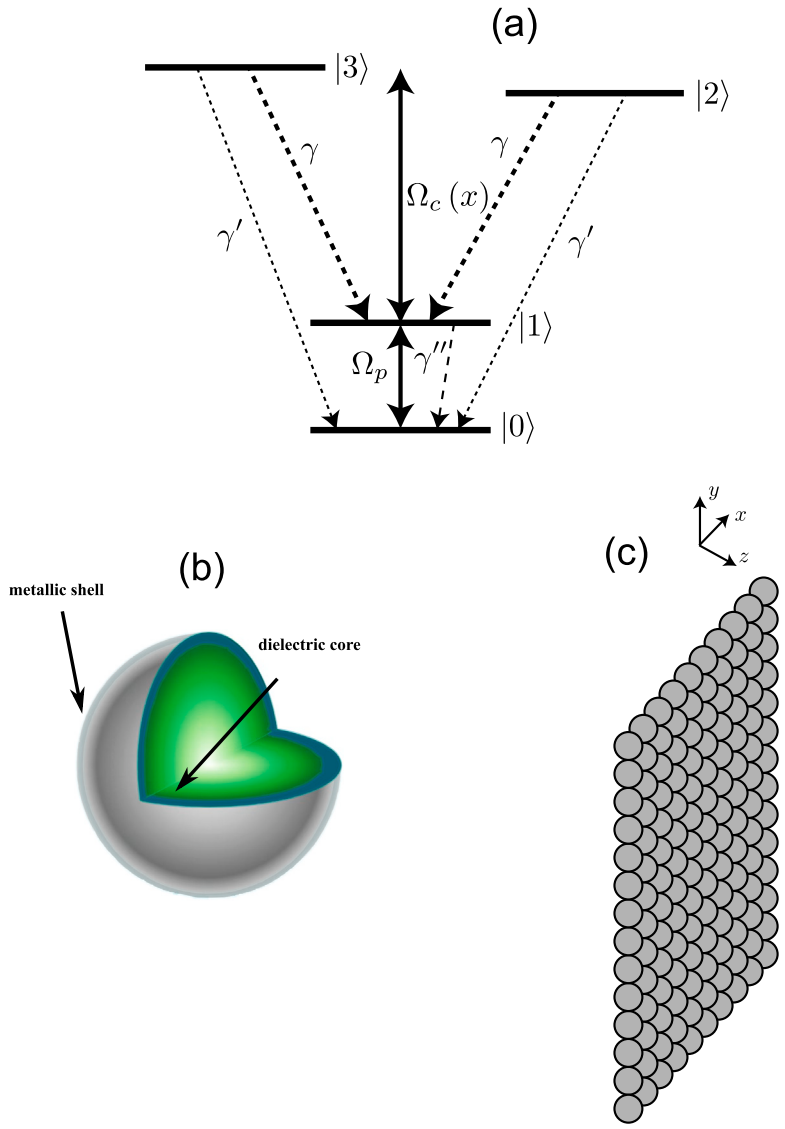

Fig. 1. A quantum system with four energy levels in ladder configuration interacting with a weak probe field as well as a strong SW control field (a). A metal-coated dielectric nanosphere (b) and a 2D array of such spheres (c).

a strong SW field, allowing to get accurate information on where the quantum emitter is localized in space. This can be achieved from the absorption distribution of the weak probe field. Interestingly, when the quantum system is situated at particular to the nanostructure, the localization is significantly improved compared to the situation in which the nanostructure is absent.

2. Model, system, equations and results

Fig. 1(a) illustrates a four-level light-matter coupling quantum system consisting of two closely lying upper states $|2\rangle$ and $|3\rangle$, as well as two lower states $|1\rangle$ and $|0\rangle$. Such a quantum system is located in vacuum with a distance d from the surface of a plasmonic nanostructure (Fig. 1(b)). More specifically, we assume that the quantum system lies on an axis normal to (the plane of) the nanostructure, crossing the center of a sphere. For example, the two upper states $|2\rangle$ and $|3\rangle$ can be Zeeman sublevels ($J = 2$, $M_J = \pm 1$), the intermediate state $|1\rangle$ can be a level with $J = 1$, $M_J = 0$, and the lower state $|0\rangle$ represent a level with $J = 0$.

The quantum system is coupled with a weak probe field characterized by the Rabi frequency $\Omega_p = \mu_{10} E_{p0}/\hbar$, as well as a strong control field of the Rabi frequency $\Omega_c = \mu E_{c0}/\hbar$. Here μ and μ_{10} are the dipole moments of the relevant transitions, and E_{p0} and E_{c0} are the electric field amplitudes. The probe laser field Ω_p drives the transition between states $|0\rangle$ and $|1\rangle$, while the control laser field Ω_c couples the state $|1\rangle$ to the states $|2\rangle$ and $|3\rangle$.

We also assume that the control field is a classical standing wave (SW) field aligned along the x direction, so the resulting Rabi-frequency of control field is given by

$$\Omega_c(x) = \Omega_c \sin(kx + \eta), \tag{1}$$

where $k = 2\pi/\lambda$ is the wave vector corresponding to the wavelength λ, while η is the phase shift of the SW beam. Assuming that the center-of mass position of the quantum system is nearly constant along the direction of the standing wave, the kinetic energy of the system can be disregarded in the interaction Hamiltonian by applying the Raman-Nath approximation [50]. The resulting Hamiltonian can be written then, in the electric dipole and rotating-wave approximations

$$H = H_0 + H_{\rm int}. \tag{2}$$

The first term in Eq. (2) describes the field-free Hamiltonian

$$H_0 = \sum_{j=0}^{3} E_j \sigma_{jj}, \tag{3}$$

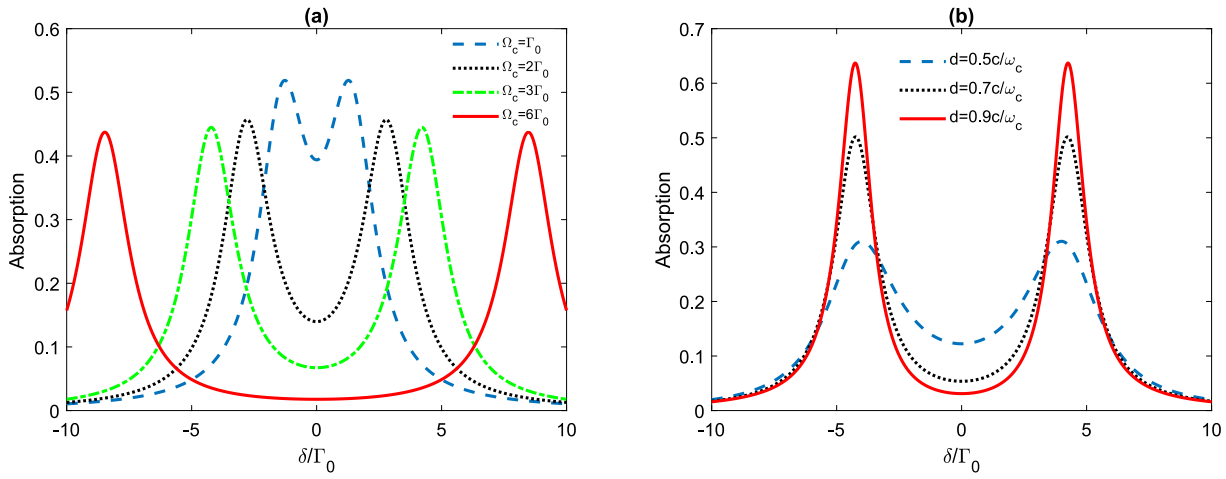

Fig. 2. The absorption spectrum [χ''] of the ladder-shaped light-matter quantum coupling (in units of $\frac{N\mu_{10}^2}{\epsilon_0\hbar}$) versus the detuning of probe field δ. (a) is when the plasmonic nanostructure is absent ($d=\infty$), while (b) is in the presence of the plasmonic nanostructure. In (a), the decay rate is Γ_0, but in (b) $\bar{\omega}=0.632\omega_p$. In (a) the spectrum is plotted for different values of the control field, i.e., $\Omega_c=\Gamma_0$ (dashed blue), $\Omega_c=2\Gamma_0$ (dotted black), $\Omega_c=3\Gamma_0$ (dashed–dotted green) and $\Omega_c=6\Gamma_0$ (red solid). In (b) the spectrum is plotted for $\Omega_c=3\Gamma_0$ and for different distances d between the emitter and the surface of the plasmonic nanostructure, i.e., $d=0.5c/\omega_p$ (dashed blue), $d=0.7c/\omega_p$ (dotted black) and $d=0.9c/\omega_p$ (red solid).

while the second term represents to the interaction Hamiltonian

$$H_{\rm int}=-\hbar\Omega_p e^{-i\delta t}|1\rangle\langle 0|-\hbar\Omega_c(x)e^{-i\Delta_c t}\left(|1\rangle\langle 2|+|1\rangle\langle 3|\right)+\text{H.c.}\,, \tag{4}$$

where $E_j=\hbar\omega_j$ is the energy of the state $|j\rangle$ and $\sigma_{jj}=|j\rangle\langle j|$. Here also $\delta=\omega_1-\omega_0-\omega$ denotes the probe field detuning and $\Delta_c=\bar{\omega}-\omega_c$ indicates the detuning from resonance, with $\bar{\omega}=(\omega_2+\omega_3)/2-\omega_1$ being the average transition energy from the excited states $|2\rangle$ and $|3\rangle$ to the state $|1\rangle$, and ω_c being the angular frequency of the control field. Two upper states are assumed to be degenerate, i.e. $E_2=E_3$ and thus $\omega_{32}=(\omega_3-\omega_2)/2=0$. Both upper states $|2\rangle$ and $|3\rangle$ are leaking spontaneously to the states $|0\rangle$ and $|1\rangle$ with the rates γ and γ', respectively. The state $|1\rangle$ decays to $|0\rangle$ with the rate γ''. The four-level emitter is selected such that transitions $|2\rangle$, $|3\rangle$ to $|1\rangle$ lie within the surface-plasmon bands of the plasmonic nanostructure, while transitions $|2\rangle$, $|3\rangle$ to $|0\rangle$ are spectrally far from the surface-plasmon bands and are not affected by the nanostructured plasmonic metasurface. We also define Γ_0 as the decay rate of the states $|2\rangle$ and $|3\rangle$ to the state $|1\rangle$ in the electromagnetic vacuum [12].

Assuming a Markovian response and by means of the Hamiltonian of Eq. (1), the following equations for the matter fields can be obtained for the density matrix elements of the quantum emitter (to the first order in the probe field)

$$\dot{\rho}_{10}=-(\gamma''+i\delta)\rho_{10}+i\Omega_c(x)\rho_{30}+i\Omega_c(x)\rho_{20}+i\Omega_p, \tag{5}$$

$$\dot{\rho}_{20}=-(\gamma+\gamma'+i\delta+i\Delta_c)\rho_{20}+i\Omega_c(x)\rho_{10}-\kappa\rho_{30}, \tag{6}$$

$$\dot{\rho}_{30}=-(\gamma+\gamma'+i\delta+i\Delta_c)\rho_{30}+i\Omega_c(x)\rho_{10}-\kappa\rho_{20}. \tag{7}$$

Eqs. (5)–(7) imply the control field to be much stronger than the probe one, keeping most of the population in the ground state $|0\rangle$, so that one can treat the probe field as a perturbation. In the above equations, κ represents the coupling coefficient between states $|2\rangle$ and $|3\rangle$ (due to the spontaneous emission in a modified anisotropic vacuum [51]). The quantum interference can take place only if the coupling parameter κ is nonzero [52]. According to [11,53], the parameters γ and κ occur due to presence of the plasmonic nanostructure and their values are given by

$$\gamma=\frac{1}{2}(\Gamma_\perp+\Gamma_\parallel), \tag{8}$$

$$\kappa=\frac{1}{2}(\Gamma_\perp-\Gamma_\parallel), \tag{9}$$

where the values of the parameters $\Gamma_\perp$ and $\Gamma_\parallel$ depend on the distance between the quantum system and the plasmonic nanostructure and can be obtained from [5].

The linear electric susceptibility characterizes well the absorption and dispersion optical properties of the weak probe field:

$$\chi(\delta)=\frac{N\mu_{10}^2}{\epsilon_0\hbar}\frac{\rho_{10}}{\Omega_p}. \tag{10}$$

Here ϵ_0 and N denote the permittivity of vacuum and the density of the quantum emitters, respectively. The coherence ρ_{10} featured in Eq. (10) can be obtained from the density matrix Eqs. (5), (6) and (7) in the steady-state

$$\begin{aligned}\rho_{10}=&\Omega_p\left[i\kappa^2-i(\gamma+\gamma'+i\delta+i\Delta_c)^2\right]\left[-2\Omega_c^2(x)(\gamma+\gamma'+i\delta+i\Delta_c)\right.\\&\left.+2\kappa\Omega_c^2(x)+\kappa^2(\gamma''+i\delta)-(\gamma''+i\delta)(\gamma+\gamma'+i\delta+i\Delta_c)^2\right]^{-1}.\end{aligned} \tag{11}$$

Substituting Eq. (11) to Eq. (10) yields

$$\begin{aligned}\chi(\delta)=&\frac{N\mu_{10}^2}{\epsilon_0\hbar}\left[i\kappa^2-i(\gamma+\gamma'+i\delta+i\Delta_c)^2\right]\left[-2\Omega_c^2(x)(\gamma+\gamma'+i\delta+i\Delta_c)\right.\\&\left.+2\kappa\Omega_c^2(x)+\kappa^2(\gamma''+i\delta)-(\gamma''+i\delta)(\gamma+\gamma'+i\delta+i\Delta_c)^2\right]^{-1}.\end{aligned} \tag{12}$$

When the ladder-shaped quantum emitter is located in the vacuum (far from the nanostructured plasmonic metasurface) and for $\Delta_c=0$, one gets

$$\chi(\delta)=\frac{N\mu_{10}^2}{\epsilon_0\hbar}\frac{i(\kappa+\gamma+\gamma'+i\delta)}{2\Omega_c^2(x)+(\gamma''+i\delta)(\kappa+\gamma+\gamma'+i\delta)}. \tag{13}$$

Now, let us study the absorption properties of the system (Fig. 2) without taking into account any spatial dependence of the control field. Note that the imaginary part χ'' of linear susceptibility, $\chi=\chi'+i\chi''$, refers to the absorption of the probe field by the system (while its real part χ' corresponds to the dispersion). As illustrated in Fig. 2(a), if the strength of the control beam is strong enough, the absorption profiles show a dip at center with two well-separated equally-strong peaks at $\delta=\pm\Omega_c\sqrt{2}$ associated with the transitions $|0\rangle\rightarrow|\pm\rangle$ (see Appendix). The presence of nanostructured metasurface modifies the intensity and width of the absorption peaks (see Fig. 2(b)). Clearly, for larger distances, the absorption is more reduced at line center, profounding the resonant transparency.

Next, by taking into consideration the spatial structure of the control SW field, we model the characteristic feature of the absorption profile. We are interested in resonant localization effects i.e., $\delta=\Delta_c=0$. Setting this into Eq. (12), this equation becomes purely imaginary, giving the absorption characteristics of the probe field

$$\chi''(0)=\frac{N\mu_{10}^2}{\epsilon_0\hbar}\frac{1}{\frac{2\Omega_c^2}{\kappa+(\gamma+\gamma')}\sin^2(kx)+\Gamma_0}, \tag{14}$$

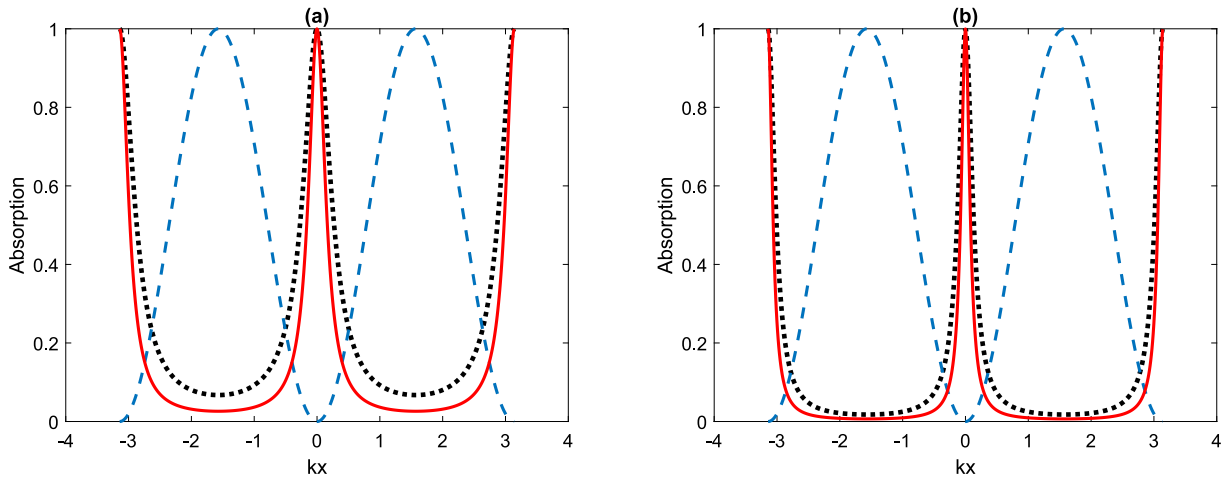

Fig. 3. The absorption spectrum [χ''] of the ladder-shaped light-matter quantum coupling (in units of $\frac{N\mu_{10}^2}{\varepsilon_0\hbar}$) versus kx for (a) $\Omega_c = 3\Gamma_0$ and (b) $\Omega_c = 6\Gamma_0$. The dotted black curve is plotted when the light-matter quantum coupling system is in vacuum, i.e., $d = \infty$, while the red solid curve is plotted when the emitter is located at a distance $d = c/\omega_p$ to the surface of nanostructure. For the simulations we selected $\Delta_c = \delta = 0$, $\gamma' = 0.3\Gamma_0$, $\eta = 0$ and $\gamma'' = \Gamma_0$. The absorption profiles are plotted in units of $\frac{N\mu_{10}^2}{\varepsilon_0\hbar}$. The dashed blue curve illustrates a sine-squared function characterizing the spatial-dependent SW field $\Omega_c(x) = \Omega_c \sin(kx + \eta)$.

where we have assumed $\gamma'' = \Gamma_0$ and $\eta = 0$. Observed in Eq. (14) the absorption peaks occur in $\chi''(0)$ at x positions satisfying $\sin^2(kx) = 0$, or $kx = n\pi$. The full width at half maximum (FWHM) of these peaks is given by

$$\Delta x = \frac{2}{k\Omega_c}\sqrt{\frac{\kappa + \gamma + \gamma'}{2}}. \tag{15}$$

If the system is in the vacuum ($\kappa = 0$), Eq. (15) takes the form

$$(\Delta x)_{\text{vacuum}} = \frac{2}{k\Omega_c}\sqrt{\frac{\Gamma_0 + \gamma'}{2}}, \tag{16}$$

while in the presence of the plasmonic nanostructure, i.e., $\kappa \neq 0$, Eq. (15) simplifies, by means of Eqs. (8) and (9)

$$(\Delta x)_{\text{plasmonic}} = \frac{2}{k\Omega_c}\sqrt{\frac{\Gamma_\perp + \gamma'}{2}}. \tag{17}$$

Clearly, the value of $\Gamma_\perp$ is the crucial parameter here. As mentioned before, $\Gamma_\perp$ values decrease with increasing the nanostructured metasurface-emitter separation. The values of $\Gamma_\perp$ are quite larger than the free-space decay rate when the emitter is very close to the surface of nanostructure. For distances up to $0.6c/\omega_p$ the value of $\Gamma_\perp$ is still larger than the corresponding decay rate values for the free-space. On the other hand, for separations between $0.65c/\omega_p$ and c/ω_p the $\Gamma_\perp$ values are less than the decay rate in vacuum. This indicates that for any metasurface-emitter separations between $0.65c/\omega_p$ and c/ω_p

$$(\Delta x)_{\text{plasmonic}} < (\Delta x)_{\text{vacuum}}, \tag{18}$$

and a superlocalization regime is achieved next to the plasmonic nanostructure.

Fig. 3 compares the localization patterns obtained from measuring the absorption of the weak probe field and for (a) $\Omega_c = 3\Gamma_0$ and (b) $\Omega_c = 6\Gamma_0$ when the ladder light-matter coupling quantum scheme is in the vacuum, i.e., $d = \infty$ (dotted black), and when it is placed in proximity to the plasmonic nanostructure (red solid). For the latter case we selected $d = c/\omega_p$ for which the value of $\Gamma_\perp$ is very small ($\Gamma_\perp = 0.183\Gamma_0$). One can see that the presence of plasmonic nanostructure produces sharper peaks on the spatial distribution of absorption profile with a better resolution, well below the diffraction limit (compared to the case which it is absent). Increasing the intensity of SW beam yields much tighter confinement of absorption peaks, as depicted in Fig. 4.

Next in Fig. 5 we illustrate how the number of subwavelength peaks, their widths and positions are modified as we vary the system parameters. When the phase shift associated with the SW beam is set to $\eta = \pi/2$, the number of localization peaks reduces to two. In this case, each absorption peak is situated in one sub-halfwavelength region ($kx = \{-\pi, 0\}$ and $kx = \{0, \pi\}$). Increasing the intensity of SW causes a stricter confinement of emitters situated next to the plasmonic nanostructure. Another regime of localization corresponds to the existence of four peaks as opposed to the three (Figs. 3 and 4) and two (Fig. 5). This can be achieved when the probe field is not on resonance $\delta \neq 0$, see Fig. 6. In such a situation, each half-subwavelength domain contains two peaks, whose position can be controlled by the phase shift parameter η.

Let us next investigate the localization in two-dimensional (2D) of the quantum emitters next to the plasmonic nanostructure. For this situation, the control field is a combination of two orthogonal standing wave fields with the same frequency

$$\Omega_c(x, y) = \Omega_c[\sin(kx + \eta_1) + \sin(ky + \eta_2)], \tag{19}$$

with $\eta_{1,2}$ being the corresponding phase shifts of the standing waves. Fig. 7 shows the 2D simulations by proper adjusting the system parameters. As shown in Fig. 7(a), when $\delta = 0, \eta_1 = \eta_2 = 0$, the absorption peaks are distributed on the diagonal in both second and fourth quadrants. The peaks of 2D localization resembles a lattice-like pattern with a uniform distribution of position probability which are across diagonals (corresponding to $kx + ky = 2m\pi$ or $kx - ky = (2n + 1)\pi$ with m, n being integers). For $\delta = 0$ but $\eta_1 = \eta_2 = \pi/2$ (Fig. 7(b)), the maxima in the absorption profile are spreaded in all four quadrants of the 2D plane and with a square-like pattern. For $\delta = 7\Gamma_0$, $\eta_1 = \eta_2 = 0$, the absorption peaks appear in the first and third quadrants with a crater-like structure. The emitter is localized at the circular edges of the two craters [see Fig. 7(c)]. Finally, for $\delta = 12\Gamma_0$, $\eta_1 = \eta_2 = 0$, the resulting spectrum of absorption represents a pattern with two spikes placed in the first and third quadrants. Such a structure provides a higher resolution in the spatial distribution of the probe absorption of the quantum emitter situated in thr vicinity of the plasmonic nanostructure.

3. Concluding remarks

In conclusion, we have investigated the distant control of localization of a four-level quantum emitter in ladder configuration adjacent to a plasmonic nanostructure. In such a light-matter coupling scheme, the upper leg interacting with a standing wave control field is affected by the surface-plasmon bands of the nanostructure, while the lower one is interacting with a weak probe beam corresponding to the free

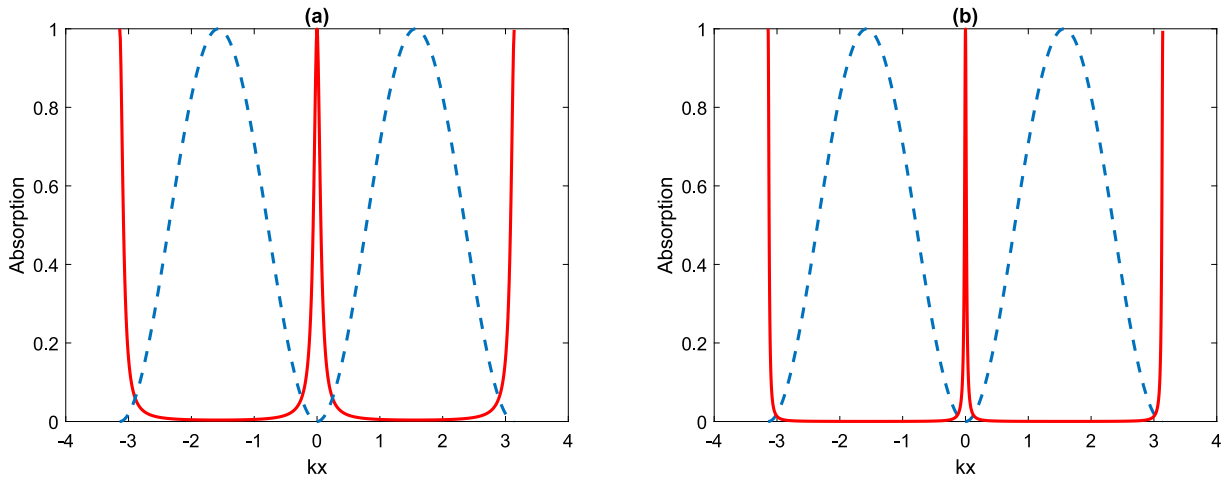

Fig. 4. The absorption spectrum $[\chi'']$ of the ladder-shaped light-matter quantum coupling (in units of $\frac{N\mu_{10}^2}{\epsilon_0\hbar}$) versus kx for (a) $\Omega_c = 8\Gamma_0$ and (b) $\Omega_c = 30\Gamma_0$ when the emitter is located at a distance $d = c/\omega_p$ to the surface of plasmonic nanostructure. For the simulations we selected $\Delta_c = \delta = 0$, $\gamma' = 0.3\Gamma_0$, $\eta = 0$ and $\gamma'' = \Gamma_0$. The absorption profiles are plotted in units of $\frac{N\mu_{10}^2}{\epsilon_0\hbar}$. The dashed blue curve illustrates a sine-squared function characterizing the spatial-dependent SW field $\Omega_c(x) = \Omega_c \sin(kx + \eta)$.

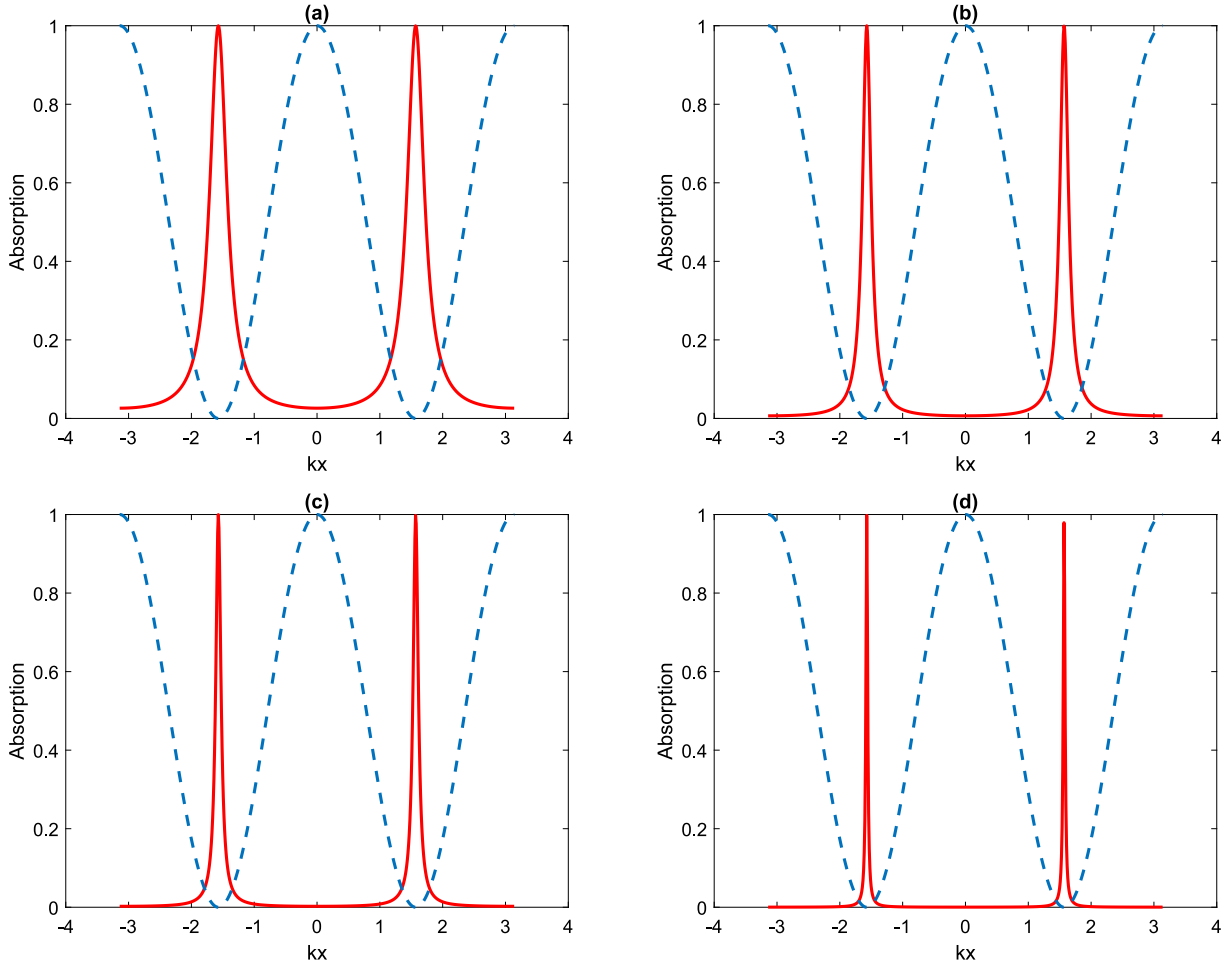

Fig. 5. The absorption spectrum $[\chi'']$ of the ladder-shaped light-matter quantum coupling (in units of $\frac{N\mu_{10}^2}{\epsilon_0\hbar}$) versus kx for (a) $\Omega_c = 3\Gamma_0$, (b) $\Omega_c = 6\Gamma_0$, (c) $\Omega_c = 10\Gamma_0$ and (d) $\Omega_c = 30\Gamma_0$ when the emitter is located at a distance $d = c/\omega_p$ to the surface of plasmonic nanostructure. For the simulations we selected $\Delta_c = \delta = 0$, $\gamma' = 0.3\Gamma_0$, $\eta = \pi/2$ and $\gamma'' = \Gamma_0$. The absorption profiles are plotted in units of $\frac{N\mu_{10}^2}{\epsilon_0\hbar}$. The dashed blue curve illustrates a sine-squared function characterizing the spatial-dependent SW field $\Omega_c(x) = \Omega_c \sin(kx + \eta)$.

space. The application of the strong SW beam makes the light-matter interaction spatially dependent. This indicates that by measuring the absorption of the weak probe field one can acquire information about the spatial location of the quantum emitter. It is found that such the quantum interference in decay channels can significantly improve the spatial confinement of quantum emitters, if the separation between the

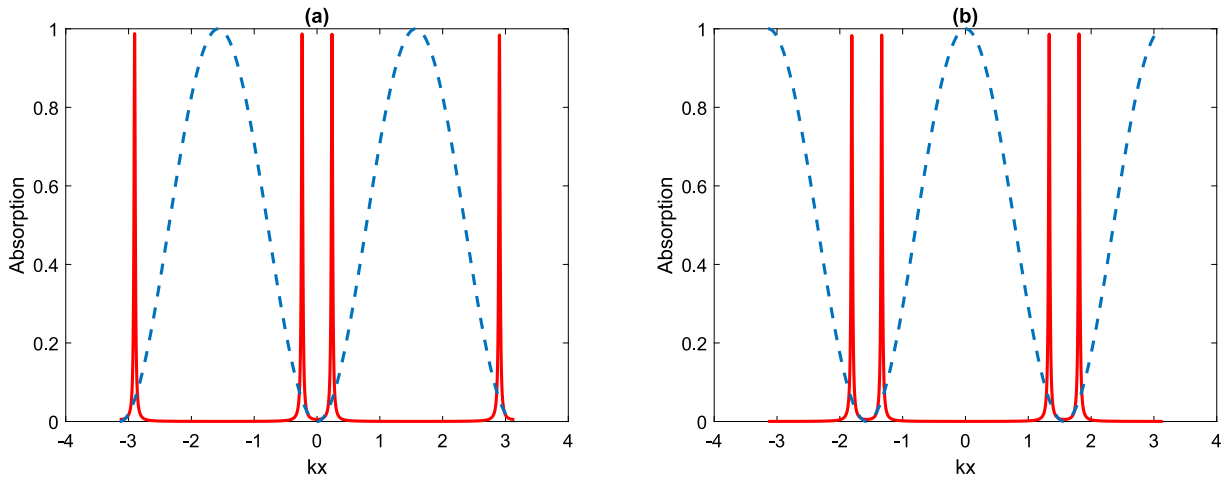

Fig. 6. The absorption spectrum $[\chi'']$ of the ladder-shaped light-matter quantum coupling in units of $\frac{N\mu_{10}^2}{\epsilon_0\hbar}$ versus kx for (a) $\delta = 10\Gamma_0$, $\eta = 0$ (b) $\delta = 10\Gamma_0$, $\eta = \pi/2$. The emitter is located at a distance $d = c/\omega_p$ to the surface of plasmonic nanostructure. For the simulations we selected $\Delta_c = 0$, $\Omega_c = 30\Gamma_0$, $\gamma' = 0.3\Gamma_0$, $\eta = \pi/2$ and $\gamma'' = 0.53\Gamma_0$. The absorption profiles are plotted in units of $\frac{N\mu_{10}^2}{\epsilon_0\hbar}$. The dashed blue curve illustrates a sine-squared function characterizing the spatial-dependent SW field $\Omega_c(x) = \Omega_c \sin(kx + \eta)$.

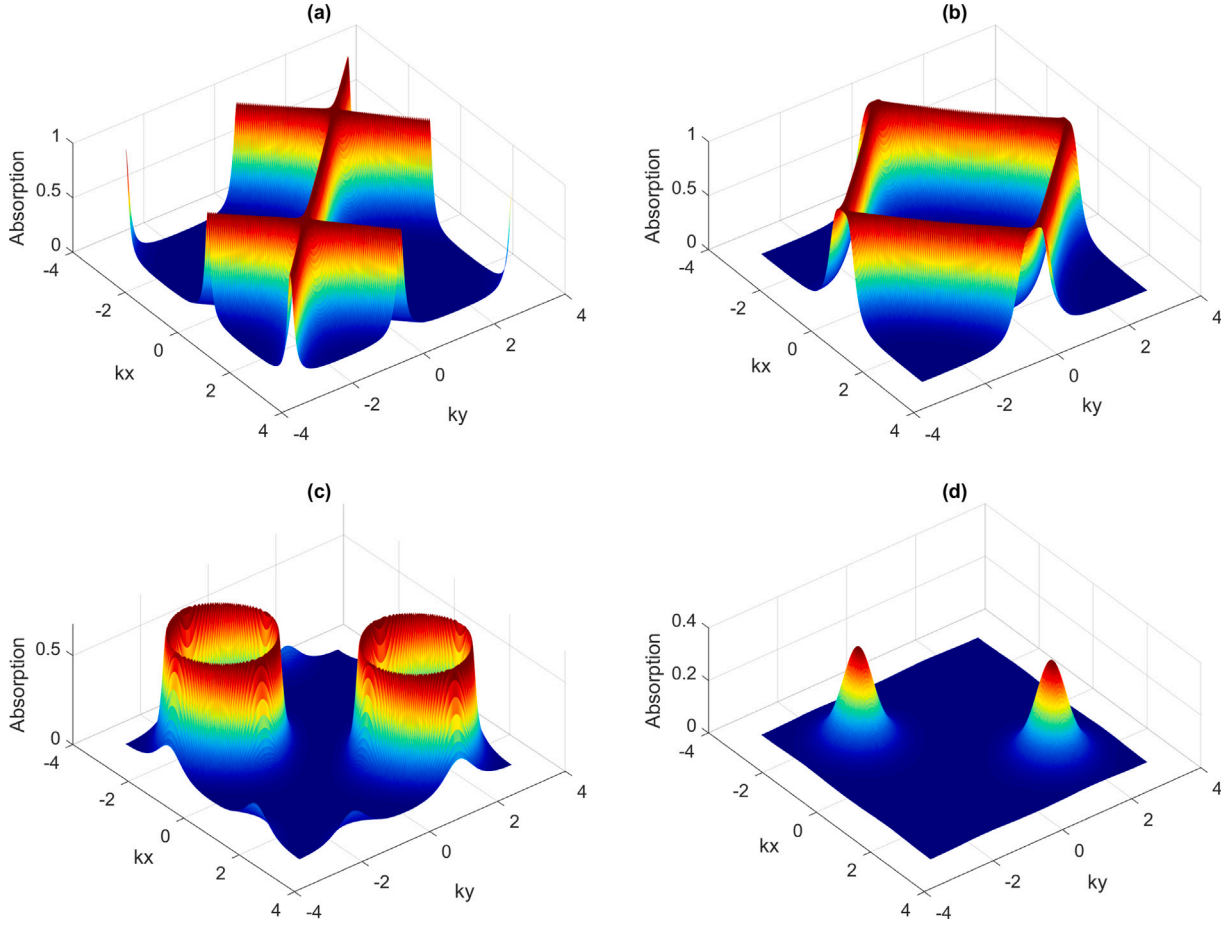

Fig. 7. The absorption spectrum $[\chi'']$ of the ladder-shaped light-matter quantum coupling (in units of $\frac{N\mu_{10}^2}{\epsilon_0\hbar}$) versus kx and ky for (a) $\delta = 0$, $\eta_1 = \eta_2 = 0$, (b) $\delta = 0$, $\eta_1 = \eta_2 = \pi/2$, (c) $\delta = 7\Gamma_0$, $\eta_1 = \eta_2 = 0$, (d) $\delta = 12\Gamma_0$, $\eta_1 = \eta_2 = 0$. The emitter is located at a distance $d = c/\omega_p$ to the surface of plasmonic nanostructure. For the simulations we selected $\Delta_c = 0$, $\gamma' = 0.3\Gamma_0$, $\Omega_c = 4\Gamma_0$ and $\gamma'' = \Gamma_0$. The absorption profiles are plotted in units of $\frac{N\mu_{10}^2}{\epsilon_0\hbar}$.

emitter and plasmonic nanostructure is between $0.65c/\omega_p$ and c/ω_p. We also studied a 2D localization of the quantum system next to the plasmonic nanostructure. Different patterns as lattices, squares, craters and spikes have been observed in the $x-y$ plane by properly adjusting the controlling parameters of the system.

Declaration of competing interest

The authors declare that they have no known competing financial interests or personal relationships that could have appeared to influence the work reported in this paper.

Data availability

Data will be made available on request.

Acknowledgments

This work was supported by the Lithuanian Research Council, Grant No. S-MIP-20-36.

Appendix

The modification of the absorption of the probe field can be understood by using the semi classical dressed state picture. Defining the rotated states $|2\rangle = e^{-i\omega_c t}|\tilde{2}\rangle$, $|3\rangle = e^{-i\omega_c t}|\tilde{3}\rangle$, $|1\rangle = |\tilde{1}\rangle$ and $|0\rangle = |\tilde{0}\rangle$, and neglecting the terms proportional to Ω_p, the total Hamiltonian in the rotated frame reads ($\hbar = 1$)

$$H_{\rm rot} = \Delta_c \left(|\tilde{2}\rangle\langle\tilde{2}| + |\tilde{3}\rangle\langle\tilde{3}|\right) - \Omega_c \left(|\tilde{3}\rangle\langle\tilde{1}| + |\tilde{2}\rangle\langle\tilde{1}| + \text{H.c.}\right). \tag{20}$$

Diagonalizing the rotated Hamiltonian one arrives at the following characteristic equation (by assuming that the ground state is not coupled to other states)

$$b^3 - a_1 b^2 + a_2 b + a_3 = 0, \tag{21}$$

where b are the eigenenergies of the Hamiltonian $a_1 = 2\Delta_c$, $a_2 = \Delta_c^2 - 2\Omega_c^2$, $a_3 = 2\Delta_c\Omega_c^2$. For $\Delta_c = 0$, we find

$$b_0 = 0, \; b_\pm = \pm\Omega_c\sqrt{2}, \tag{22}$$

with the normalized eigenstates

$$|D\rangle = \frac{|\tilde{2}\rangle - |\tilde{3}\rangle}{\sqrt{2}}, \tag{23}$$

$$|\pm\rangle = \frac{1}{\sqrt{2}}\left(|\tilde{1}\rangle \mp \frac{|\tilde{2}\rangle + |\tilde{3}\rangle}{\sqrt{2}}\right). \tag{24}$$

Clearly, eigenstates show that $|0\rangle$ cannot be coupled to $|D\rangle$ as there is no contribution of $|1\rangle$.

References

[1] C. Lienau, M.A. Noginov, M. Loncar, Light–matter interactions at the nanoscale, J. Opt. 16 (2014) 110201.
[2] J.N. Anker, W.P. Hall, O. Lyandres, N.C. Shah, J. Zhao, R.P.V. Duyne, Biosensing with plasmonic nanosensors, Nature Mater. 7 (2008) 442–453.
[3] M.I. Stockman, Nanoplasmonics: past, present, and glimpse into future, Opt. Express 19 (2011) 22029–22106.
[4] B. Sharma, R. R.Frontiera, A.-I. Henry, E. Ringe, R.P. Duyne, SERS: Materials, applications, and the future, Mater. Today 15 (2012) 16–25.
[5] S. Evangelou, V. Yannopapas, E. Paspalakis, Transparency and slow light in a four-level quantum system near a plasmonic nanostructure, Phys. Rev. A 86 (2012) 053811.
[6] J. Li, S. Shen, C. Ding, Y. Wu, Magnetically induced optical transparency in a plasmon-exciton system, Phys. Rev. A 103 (2021) 053706.
[7] L. Wang, Y. Gu, H. Chen, J.-Y. Zhang, Y. Cui, B. Gerardot, Q.-H. Gong, Polarized linewidth-controllable double-trapping electromagnetically induced transparency spectra in a resonant plasmon nanocavity, Sci. Rep. 3 (2013) 2879.
[8] Z.-P. Wang, B.-L. Yu, Plasmonic control of refractive index without absorption in metallic photonic crystals doped with quantum dots, Plasmonics 13 (2018) 567.
[9] R.D. Artuso, G.W. Bryant, Strongly coupled quantum dot-metal nanoparticle systems: Exciton-induced transparency, discontinuous response, and suppression as driven quantum oscillator effects, Phys. Rev. B 82 (2010) 195419.
[10] W. Zhang, A.O. Govorov, G.W. Bryant, Semiconductor-metal nanoparticle molecules: Hybrid excitons and the nonlinear Fano effect, Phys. Rev. Lett. 97 (2006) 146804.
[11] V. Yannopapas, E. Paspalakis, N.V. Vitanov, Plasmon-induced enhancement of quantum interference near metallic nanostructures, Phys. Rev. Lett. 103 (2009) 063602.
[12] S. Evangelou, V. Yannopapas, E. Paspalakis, Modifying free-space spontaneous emission near a plasmonic nanostructure, Phys. Rev. A 83 (2011) 023819.
[13] Y. Gu, L. Wang, P. Ren, J. Zhang, T. Zhang, O.J.F. Martin, Q. Gong, Surface-plasmon-induced modification on the spontaneous emission spectrum via subwavelength-confined anisotropic purcell factor, Nano Lett. 12 (2012) 2488.
[14] A.V. Malyshev, V.A. Malyshev, Optical bistability and hysteresis of a hybrid metal-semiconductor nanodimer, Phys. Rev. B 84 (2011) 035314.
[15] F. Carreno, M.A. Anton, E. Paspalakis, Nonlinear optical rectification and optical bistability in a coupled asymmetric quantum dot-metal nanoparticle hybrid, J. Appl. Phys. 124 (2018) 113107.
[16] H.R. Hamedi, E. Paspalakis, V. Yannopapas, Effective control of the optical bistability of a three-level quantum emitter near a nanostructured plasmonic metasurface, Photonics 8 (7) (2021) 285.
[17] J.-B. Li, N.-C. Kim, M.-T. Cheng, L. Zhou, Z.-H. Hao, Q.-Q. Wang, Optical bistability and nonlinearity of coherently coupled exciton-plasmon systems, Opt. Express 20 (2012) 1856.
[18] S.K. Singh, M.K. Abak, M.E. Tasgin, Enhancement of four-wave mixing via interference of multiple plasmonic conversion paths, Phys. Rev. B 93 (2016) 035410.
[19] H. Chen, J. Ren, Y. Gu, D. Zhao, J. Zhang, Q. Gong, Nanoscale Kerr nonlinearity enhancement using spontaneously generated coherence in plasmonic nanocavity, Sci. Rep. 5 (2016) 18315.
[20] H.R. Hamedi, V. Yannopapas, A. Mekys, E. Paspalakis, Control of Kerr nonlinearity in a four-level quantum system near a plasmonic nanostructure, Physica E 130 (2021) 114662.
[21] S.M. Sadeghi, Gain without inversion in hybrid quantum dot–metallic nanoparticle systems, Nanotechnology 21 (2010) 455401.
[22] D. Zhao, Y. Gu, J. Wu, J. Zhang, T. Zhang, B.D. Gerardot, Q. Gong, Quantum-dot gain without inversion: Effects of dark plasmon-exciton hybridization, Phys. Rev. B 89 (2014) 245433.
[23] F. Carreño, M.A. Antón, V. Yannopapas, E. Paspalakis, Control of the absorption of a four-level quantum system near a plasmonic nanostructure, Phys. Rev. B 95 (2017) 195410.
[24] M.R. Singh, Enhancement of the second-harmonic generation in a quantum dot–metallic nanoparticle hybrid system, Nanotechnology 24 (2014) 125701.
[25] P.K. Jha, Y. Wang, X. Ren, X. Zhang, Quantum-coherence-enhanced transient surface plasmon lasing, J. Opt. 19 (2017) 054002.
[26] S.H. Asadpour, A. Panahpour, M. Jafari, Phase-dependent electromagnetically induced grating in a four-level quantum system near a plasmonic nanostructure, Eur. Phys. J. Plus 133 (411) (2018).
[27] M.G.G. Abad, M. Mahmoudi, Atom-photon entanglement near a plasmonic nanostructure, Eur. Phys. J. Plus 135 (352) (2020).
[28] K. Staliunas, S. Longhi, G.J. de Valcárcel, Faraday patterns in Bose-Einstein condensates, Phys. Rev. Lett. 89 (2002) 210406.
[29] W.D. Phillips, Nobel lecture: Laser cooling and trapping of neutral atoms, Rev. Modern Phys. 70 (1998) 721–741.
[30] J. Evers, S. Qamar, M.S. Zubairy, Atom localization and center-of-mass wave-function determination via multiple simultaneous quadrature measurements, Phys. Rev. A 75 (2007) 053809.
[31] K.S. Johnson, J.H. Thywissen, N.H. Dekker, K.K. Berggren, A.P. Chu, R. Younkin, M. Prentiss, Localization of metastable atom beams with optical standing waves: Nanolithography at the Heisenberg limitlocalization of metastable atom beams with optical standing waves: Nanolithography at the Heisenberg limit, Science 280 (1998) 1583.
[32] M. Sahrai, H. Tajalli, K.T. Kapale, M.S. Zubairy, Subwavelength atom localization via amplitude and phase control of the absorption spectrum, Phys. Rev. A 72 (2005) 013820.
[33] E. Paspalakis, P.L. Knight, Localizing an atom via quantum interference, Phys. Rev. A 63 (2001) 065802.
[34] Rahmatullah, S. Qamar, Two-dimensional atom localization via probe-absorption spectrum, Phys. Rev. A 88 (2013) 013846.
[35] C. Ding, J. Li, X. Yang, D. Zhang, H. Xiong, Proposal for efficient two-dimensional atom localization using probe absorption in a microwave-driven four-level atomic system, Phys. Rev. A 84 (2011) 043840.
[36] H.R. Hamedi, G. Juzeliūnas, Phase-sensitive atom localization for closed-loop quantum systems, Phys. Rev. A 94 (2016) 013842.
[37] G.S. Agarwal, K.T. Kapale, Subwavelength atom localization via coherent population trapping, J. Phys. B: At. Mol. Opt. Phys. 39 (2006) 3437.
[38] V.S. Ivanov, Y.V. Rozhdestvensky, K.-A. Suominen, Three-dimensional atom localization by laser fields in a four-level tripod system, Phys. Rev. A 90 (2014) 063802.
[39] Z. Wang, J. Jiang, Sub-half-wavelength atom localization via probe absorption spectrum in a four-level atomic system, Phys. Lett. A 374 (2010) 4853–4858.
[40] Z. Wang, T. Shui, B. Yu, Efficient two-dimensional atom localization in a four-level atomic system beyond weak-probe approximation, Opt. Commun. 313 (2014) 263–269.
[41] H. Xu, Phase control of two-dimensional probe gain-absorption spectra in semiconductor quantum wells, Physica E 69 (2015) 186–190.
[42] N.A. Proite, Z.J. Simmons, D.D. Yavuz, Observation of atomic localization using electromagnetically induced transparency, Phys. Rev. A 83 (2011) 041803.
[43] J. Mompart, V. Ahufinger, G. Birkl, Coherent patterning of matter waves with subwavelength localization, Phys. Rev. A 79 (2009) 053638.
[44] J.A. Miles, Z.J. Simmons, D.D. Yavuz, Subwavelength localization of atomic excitation using electromagnetically induced transparency, Phys. Rev. X 3 (2013) 031014.

[45] Z. Wang, B. Yu, J. Zhu, Z. Cao, S. Zhen, X. Wu, F. Xu, Atom localization via controlled spontaneous emission in afive-level atomic system, Ann. Phys. 327 (2012) 1132–1145.
[46] H.R. Hamedi, G. Zlabys, V. Ahufinger, T. Halfmann, J. Mompart, G. Juzeliunas, Spatially strongly confined atomic excitation via a two dimensional stimulated Raman adiabatic passage, Opt. Express 30 (2022) 13915–13930.
[47] J. Xu, Q. Li, W. chao Yan, X. dong Chen, X. ming Hu, Sub-half-wavelength localization of a two-level atom via trichromatic phasemanipulation, Phys. Lett. A 372 (2008) 6032.
[48] H.R. Hamedi, G. Zlabys, V. Ahufinger, T. Halfmann, J. Mompart, G. Juzeliunas, Spatially strongly confined atomic excitation via a two dimensional stimulated Raman adiabatic passage, Opt. Express 30 (2022) 13915–13930.
[49] M. Idrees, M. Ullah, B.A. Bacha, A. Ullah, L.-G. Wang, High–resolution two–dimensional atomic localization via tunablesurface plasmon polaritons, Plasmonics 16 (2021) 1773–1780.
[50] P. Meystre, Atom Optics, Springer, New York, NY, 2001.
[51] G.S. Agarwal, Anisotropic vacuum-induced interference in decay channels, Phys. Rev. Lett. 84 (2000) 5500–5503.
[52] M. Kiffner, M. Macovei, J. Evers, C.H. Keitel, Chapter 3 - Vacuum-induced processes in multilevel atoms, Prog. Opt. 55 (2010) 85.
[53] S. Evangelou, V. Yannopapas, E. Paspalakis, Simulating quantum interference in spontaneous decay near plasmonic nanostructures: Population dynamics, Phys. Rev. A 83 (2011) 055805.